

pubs.acs.org/IECR Article

Understanding and Optimizing the Behavior of Al- and Ru-Based Catalysts for the Synthesis of Polyisobutenyl Succinic Anhydrides

Cristian A. Morales-Rivera, Glenn Cormack, James Burrington, Nicolas Proust, and Giannis Mpourmpakis*



Cite This: Ind. Eng. Chem. Res. 2022, 61, 14462-14471



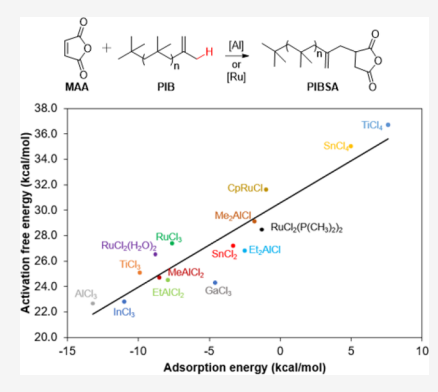
ACCESS I

III Metrics & More

Article Recommendations

s Supporting Information

ABSTRACT: Polyisobutenyl succinic anhydrides (PIBSAs) are an important class of chemicals in the automotive industry due to their wide use in lubricant and fuel formulations. However, the synthesis of these molecules takes place at elevated temperatures through the ene reaction between maleic anhydride (MAA) and polyisobutylene (PIB). Lewis acid catalysts (e.g., AlCl₃) have been shown to facilitate PIBSA synthesis by lowering the activation energy of the reaction; however, the desorption of the final product (PIBSA) from the catalyst can be highly endergonic. Herein, we demonstrate ligand engineering strategies to optimize the performance of Aland Ru-based catalysts by combining first-principles calculations with kinetic modeling. We discover that alkyl chlorides such as the EtAlCl₂ retain relatively low activation barriers like AlCl₃, while lowering the desorption energy of the final product (PIBSA). In addition, we address metal oxidation state and ligand effects on the ene reaction performance of Ru-based catalysts. We demonstrate that depending on the metal



oxidation state and type of ligands there is a competition between concerted and stepwise mechanisms. We uncover a Ru(II) catalyst, $RuCl_2 \cdot 2H_2O$, exhibiting enhanced activity but suffering from low stability. Overall, our work identifies catalysts of industrial importance that can reduce the energy input required for intensified processes and highlights challenges associated with catalyst performance.

1. INTRODUCTION

Polyisobutenyl succinic anhydrides (PIBSAs) and their succinimide (PIBSI) derivatives are important chemicals in the automotive industry due to their use as detergentdispersant additives in lubricant and fuel formulations. They are commonly synthesized through the ene reaction between maleic anhydride (MAA) and polyisobutylene (PIB).^{2,3} However, the reaction conditions require elevated temperatures, making the overall process energy intense.3 Lewis acids are known to be effective catalysts for ene type reactions by interacting with the enophile and making it more electrondeficient.^{4,5} In our recent computational work,⁶ based on density functional theory (DFT) calculations, we demonstrated that Lewis acids are potential catalyst for the ene reaction between MAA and PIB, making the reaction kinetically more favorable compared to the uncatalyzed reaction. Detailed mechanistic studies revealed that the reaction proceeds through a concerted mechanism (Scheme 1). In addition, turnover frequency (TOF) calculations from kinetic modeling using the energy span model⁷ revealed AlCl₃ (among other Lewis acids) to be the most active catalyst due to its acidic strength. Importantly, this study also revealed that even though stronger Lewis acids will favor adsorption (i.e., binding) of MAA and will lower the activation energy of the reaction, the desorption (i.e., release) of PIBSA from the

Scheme 1. Plausible Mechanism for the Lewis Acid (LA) Catalyzed Ene Reaction between MAA and PIB as Suggested by DFT Calculations⁶

Received: June 8, 2022
Revised: August 16, 2022
Accepted: September 13, 2022
Published: September 22, 2022





catalyst will be disfavored (Scheme 1) due to strong catalyst—PIBSA interactions.

Aluminum-based Lewis acid catalysts have been shown to be active for a variety of reactions of industrial importance. For example, alumina has been shown to selectively activate C-H bonds of alkanes due to its inherent Lewis acidity (metal centers) and basicity (oxygen centers).8 This nonoxidative alkane dehydrogenation has been shown to be a promising route to produce olefins that are commonly used as building blocks in the chemical industry to produce commodity chemicals such as polymers, plastics, and petrochemicals. In addition to aluminum oxides, alkylaluminum chlorides have been shown to effectively catalyze ene type reactions. ¹⁰ The set of RAICl₂, R₂AICl₂ and R₃Al provides a series of Lewis acid catalyst of gradually decreasing acidity.⁴ EtAlCl₂, for example, has been shown to catalyze the ene reaction involving α,β unsaturated esters as the enophile.¹¹ On the other hand, Me₂AlCl acts as catalyst in the ene reaction between $\alpha_1\beta_2$ unsaturated aldehydes/ketones¹² and saturated aldehydes.^{4,13}

In addition to Al-based catalyst, Ru-based catalysts have been also shown to catalyze ene reactions. 14-18 Ru(III) catalyst (RuCl₃), for example, was reported to catalyze the ene reaction between MAA and polypropylene containing a vinylidene end group. 19 For this reaction, a 9.7 mol % of MAA incorporation was obtained at 240 °C, using 0.05% mol catalyst/mol MAA and 2.7 mol MAA/mol vinylidene. On the other hand, Ru(0) catalyzed the ene reaction between maleimides and alkenes to form alkylidene succinimide derivatives. 17 These reactions proceed with high yield percentage of the desirable product. However, the reactions require α,β -unsaturated carbonyl partners bearing electron withdrawing groups. In addition, Ru(II) catalysts have been shown to be active catalysts for cross coupling, hydrogentransfer, and Alder-ene reactions. 16,18,20 Computational and experimental studies have suggested that the ene reaction catalyzed by Ru catalysts will proceed through a coordination, stepwise mechanism involving oxidative addition, H-elimination, and reductive elimination steps as shown in Scheme

Despite the aforementioned studies, the effects of ligands and oxidation state of the catalyst metal center on the ene reaction involving MAA and PIB have not been well

Scheme 2. Proposed Stepwise Mechanism for the Ru Catalyzed Ene Reaction between MAA and PIB^a

understood. This knowledge gap currently hinders the discovery of novel ene-type catalysts that can effectively incorporate MAA into PIB and thus limits any efforts to optimize this energy intense industrial process. Herein, we investigated how ligand engineering can optimize the performance of Al-based catalysts and alter catalytic behavior of Ru catalysts through modulating the oxidation state of the active center. We found that the selection of ligands in Al-based catalysts can lower the desorption energy of the final product (PIBSA) while keeping a reduced activation energy of the ratedetermining step. In addition, we demonstrated that the mechanism can change from a concerted to a stepwise on Ru catalysts with the Ru(II) complexes being more active. However, the stability of Ru(II) catalysts under experimental conditions may be a challenge. This computational work sheds light into the complexity of ene reactions and can aid the discovery of new Lewis acid catalysts for reactions of industrial importance (i.e., PIBSA formation).

2. COMPUTATIONAL DETAILS

All calculations were performed with the program package Gaussian 09.²³ Images of the 3D molecular structures were generated using CYLview.²⁴ The geometries of all intermediates and transition states were optimized using the M06-2X functional and the 6-31G(d) basis set. Single point energy calculations were performed with M06-2X²⁵ and the 6-311+G(d,p) basis set. The SDD pseudopotential basis set was used for ruthenium atoms. Thermal corrections to the Gibbs free energies and enthalpies were calculated using the harmonic oscillator approximation at 423.15 K (simulating experimental conditions). Frequency calculations were performed to confirm that each stationary point is either a minimum or a transition state. Intrinsic reaction coordinate²⁶ (IRC) calculations were used to confirm the path connection between reactants, products, and transition states. All energies in the reaction energy profiles are with respect to the reactants in infinite separation. Each structure reported is the lowest energy conformer as indicated by the calculations. Turnover frequencies (TOF) of the catalysts were calculated using the energy span model. Distortion/interaction energy analysis was performed to rationalize the catalytic activity behavior based on ligand effects. 27,28

3. RESULTS AND DISCUSSION

3.1. Catalytic Activity of Different Al-Based Acid Catalysts. In our previous computational work, we identified AlCl₃ to be the most active catalyst among a set of Lewis acid catalysts. However, the desorption of the final product from AlCl₃ was found to be highly endergonic, potentially limiting catalytic turnover due to poisoning.⁶ We expand on our previous study to explore ligand effects of Al-based catalysts as a means to decrease the desorption energy of PIBSA in the ene reaction between MAA and PIB. EtAlCl₂ catalyst was first explored taking in consideration the concerted mechanism as shown in Scheme 1 (most favorable pathway as shown by calculations). Due to its computational cost, PIB was simulated with trimethylpentene (TMP), a smaller substrate exhibiting a vinylidene double bond. The computed activation energies and reaction energies are shown in Figure 1. The overall exothermicity of the studied reaction is -9.3 kcal/mol in Gibbs free energy. The first step of the reaction energy profile (Figure 1) is the adsorption of MAA on EtAlCl₂ (state 2)

^aRuLn denotes the catalyst, where L stands for ligand.

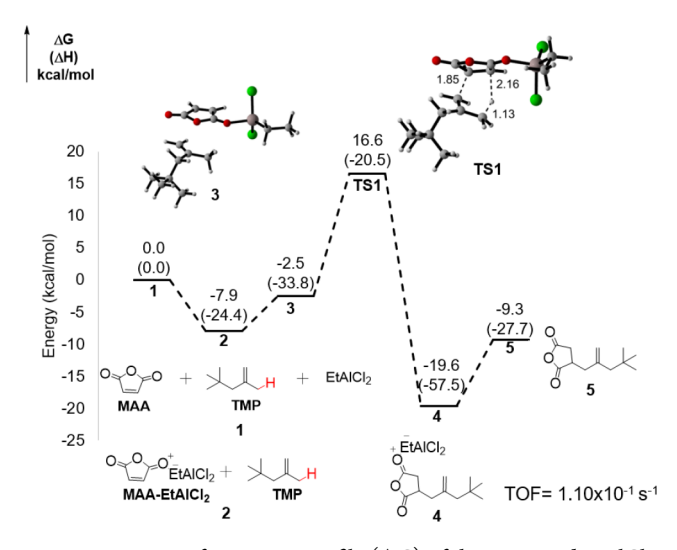


Figure 1. Reaction free energy profile (ΔG) of the concerted $EtAlCl_2$ -catalyzed ene reaction mechanism between MAA and TMP. All energies are reported in kcal/mol. The values in parentheses correspond to reaction enthalpies (ΔH) . Distances shown on the TS complex are in Å and correspond to bonds being broken or formed at the TS along the reaction path.

followed by the formation of the reactant complex 3. The activation Gibbs free energy for the concerted mechanism was calculated to be 24.5 kcal/mol (energy difference between TS1 and state 2 in Figure 1). In our previous computational study, we reported that the uncatalyzed ene reaction between MAA and TMP will proceed through a concerted mechanism requiring an activation Gibbs free energy of 36.6 kcal/mol. Thus, with EtAlCl₂ requiring a barrier of $\Delta G^{\ddagger} = 24.5 \text{ kcal/mol}$, it becomes clear that the EtAlCl2 catalyst will accelerate the incorporation of MAA to TMP, making the reaction kinetically more favorable. To further test the catalytic activity of EtAlCl₂, TOF calculations were performed by applying the energetic span model,⁷ obtaining a value of 1.10×10^{-1} s⁻¹ (Figure 1). When this result is compared to the TOF of AlCl₃ $(4.60 \times$ 10⁻¹ s⁻¹), the most active Lewis acid catalyst reported in our previous study,6 it can be observed that EtAlCl₂ catalyst has similar activity to AlCl₃. In addition, the desorption energy of product 5 from EtAlCl₂ is 10.3 kcal/mol (Figure 1), whereas the equivalent desorption step on AlCl₃ was calculated at 16.2 kcal/mol. Thus, EtAlCl₂ exhibits comparable catalytic activity to AlCl₃ and additionally has lower desorption energy of the final product. Altogether these results suggest that the EtAlCl₂ can be a potential catalyst for the ene reaction between MAA and PIB with a catalytic activity similar to AlCl₃ but with a less endothermic desorption energy of the final product.

To further explore the catalytic activity of different Al-based Lewis acid catalysts on the ene reaction between MAA and PIB, we calculated the kinetic (ΔG^{\ddagger} , ΔH^{\ddagger} , δE , TOF) and thermodynamic ($\Delta G_{\rm adsorption}$ and $\Delta G_{\rm desorption}$) data considering the concerted mechanism (most favorable pathway as shown by Morales-Rivera et al.⁶). The computed kinetic and thermodynamic information is presented in Table 1. Different alkylaluminum chloride (MeAlCl₂, Me₂AlCl, Et₂AlCl) catalysts were explored (see Supporting Information for energy profiles). Calculations showed that all Al-based Lewis acids studied will accelerate the incorporation of MAA into TMP by lowering the activation energy when compared to the uncatalyzed ene reaction (36.6 kcal/mol). Among the Al-

Table 1. Activation (ΔG^{\ddagger}) , Adsorption/Desorption (ΔG^{\ddagger}) Free Energy, Energy Span $(\delta E$, for Energy Span Model Analysis), and TOFs of the Ene Reaction between MAA and TMP, Catalyzed by Different Al-Based Lewis Acid Catalysts^a

Lewis acid	ΔG^{\ddagger}	ΔG , adsorption	ΔG , desorption	δE	TOF (s ⁻¹)
AlCl ₃	22.7	-13.2	16.2	25.7	4.60×10^{-1}
$EtAlCl_2$	24.5	-7.9	10.3	26.9	1.10×10^{-1}
$MeAlCl_2$	24.7	-8.5	11.0	27.2	7.72×10^{-2}
Et ₂ AlCl	26.8	-2.5	4.1	28.4	1.85×10^{-2}
Me ₂ AlCl	29.1	-1.8	5.2	32.5	1.41×10^{-4}

^aAll energies are in kcal/mol. AlCl₃ data are taken from literature.

based Lewis catalysts studied, $EtAlCl_2$ and $MeAlCl_2$ favor the reaction the most with an activation Gibbs free energy of 24.5 and 24.7 kcal/mol, respectively. In addition, $EtAlCl_2$ (1.10 × 10^{-1} s⁻¹) and $MeAlCl_2$ (7.72 × 10^{-2} s⁻¹) exhibit similar catalytic activity to $AlCl_3$ (4.60 × 10^{-1} s⁻¹) in terms of TOFs. However, even though $EtAlCl_2$ and $MeAlCl_2$ exhibit comparable TOF to $AlCl_3$, there is a lower desorption energy of the final product 5 from $EtAlCl_2$ and $MeAlCl_2$ (10.3 and 11.0 kcal/mol, respectively) when compared to $AlCl_3$ (16.2 kcal/mol). Altogether these results suggest that alkylaluminum chlorides can be alternative catalysts for the ene reaction between MAA and PIB by making the reaction more kinetically favorable. Specifically, $EtAlCl_2$ and $EtAlCl_3$ but with a less endothermic desorption energy of the final product.

3.2. Origin of Catalytic Activity of Al-Based Catalysts. To further understand the origin of the catalytic activity difference between all Al-based Lewis acid catalysts studied, the distortion/interaction energy analysis was performed on the concerted TSs for the ene reaction between MAA and TMP (Figure 2). This analysis examines the rigidity of the original reactants and catalysts, the extent of their deformation during the reaction, and their ability to interact as the reaction proceeds. The $\Delta E_{\text{d-total}}$ (distortion energy) is the energy required to distort the reactants and the catalyst from the ground state geometries to the configuration they adopt at the TS. On the other hand, the ΔE_{int} (interaction energy) accounts

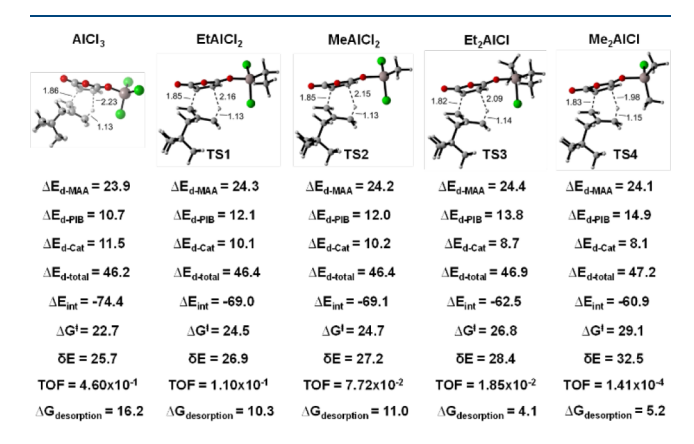


Figure 2. Distortion/interaction energy analysis on the concerted transition states of the ene reaction between MAA and TMP catalyzed by Al-based catalysts, with varying alkyl to Cl ligands. All energies are reported in kcal/mol. Distances shown on the TS complexes are in Å and correspond to bonds being broken or formed at the TS along the reaction path.

for all chemical interactions between the distorted reactants and the catalyst. The distortion energies of individual reactants and catalysts, the total distortion (of formed complexes, $\Delta E_{\text{d-total}}$), and the interaction energies for the different Albased Lewis acid catalysts are shown in Figure 2. We observe that the $\Delta E_{d-total}$ values of the concerted TSs catalyzed by different Al catalysts are very similar. However, the $\Delta E_{\rm int}$ can vary. For example, by comparing $\Delta E_{\rm int}$ of AlCl₃ (-74.4 kcal/ mol) and EtAlCl₂ (-69.0 kcal/mol), a more favorable interaction energy is observed in AlCl₃ resulting in lower activation Gibbs free energy (22.7 vs 24.5 kcal/mol respectively). If ΔE_{int} of EtAlCl₂ and MeAlCl₂ are compared, these are similar, resulting in a similar activation Gibbs free energy (24.5 vs 24.7 kcal/mol, respectively). However, if we replace one chlorine atom by an ethyl or methyl group as in the cases of Et₂AlCl and Me₂AlCl, a decrease in the interaction energy is observed (values become less exothermic) resulting in a higher activation Gibbs free energy (26.8 and 29.1 kcal/ mol, respectively). Thus, this analysis demonstrates that the difference in catalytic activity between the Al-based catalysts is due to the acid strength of the catalyst, which in turn is depicted in the interaction energy (ΔE_{int} values).

As previously mentioned, replacing one chlorine atom by an ethyl or methyl group will reduce the acidity of the catalyst, reducing the catalytic activity of the ene reaction between MAA and PIB. To explore possible steric effects that may impact the catalytic activity of Al-based Lewis acid catalysts, we investigated the (C(CH₃)₃)AlCl₂ and (C(CH₃)₃)₂AlCl catalysts as well. The distortion/interaction energy analysis was also applied to compare the catalytic activity of $(C(CH_3)_3)$ - $AlCl_2$ and $(C(CH_3)_3)_2AlCl$ to $EtAlCl_2$ and Et_2AlCl_3 respectively (keeping the number of chlorine ligands the same but changing the size of the alkyl ligand). The distortion energies of reactants and catalysts, the total distortion, and the interaction energies are shown in Figure 3. The $\Delta E_{\text{d-total}}$ values of the concerted TS catalyzed by different Al-based catalysts remain practically the same, indicating that the difference in catalytic activity between the catalysts may not be due to steric effects. However, when the $\Delta E_{\rm int}$ are compared, a significant difference is observed indicating that the catalytic activity

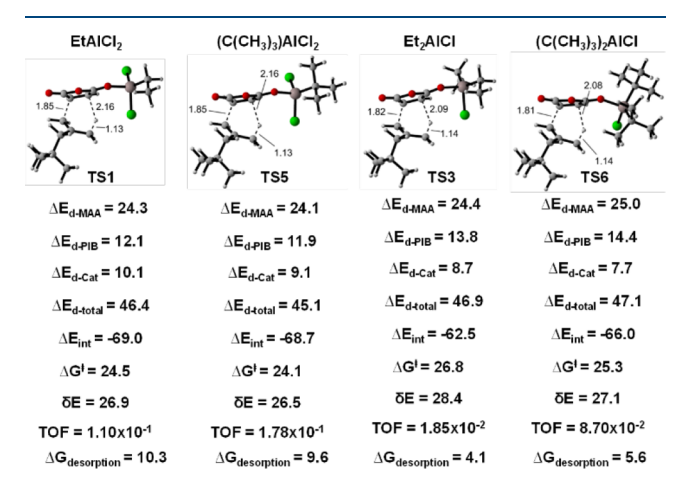


Figure 3. Distortion/interaction energy analysis on the concerted transition states of the ene reaction between MAA and TMP catalyzed by Al-based catalysts with varying alkyl size. All energies are reported in kcal/mol. Distances shown on the TS complexes are in Å and correspond to bonds being broken or formed at the TS along the reaction path.

behavior is still due to the acid strength of the catalyst. We note that the selection of TMP to simulate PIB (to reduce computational cost) may underestimate steric effects. However, the relatively small size of the studied (molecular) catalysts and the MAA, which directly coordinates with the catalyst, as well as the systematic comparison of the catalysts, give confidence that the acid strength, depicted in the $\Delta E_{\rm intr}$ is the driving descriptor for the observed catalytic trends. As we show for the Ru(II) complexes (*vide infra*), steric effects can play an important role in the catalyst reactivity.

3.3. Effect of Oxidation State of Ru-Based Catalysts. We next investigated the effect of oxidation state of Ru-based catalyst on the ene reaction between MAA and PIB. The stepwise mechanism involving an oxidative addition, H-migration, and reductive elimination steps, catalyzed by Ru(III) (RuCl₃), ¹⁹ was first studied (Figure 4, black path).

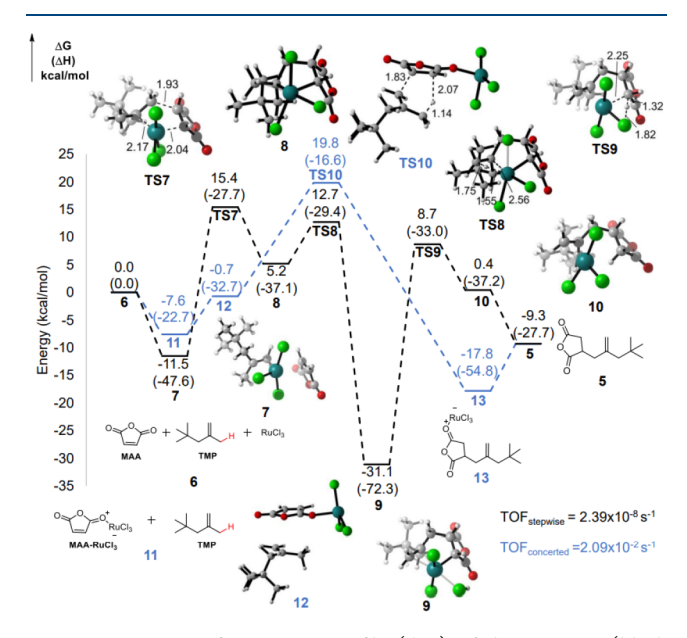


Figure 4. Reaction free energy profile (ΔG) of the stepwise (black path) and concerted (blue path) RuCl₃ catalyzed ene reaction mechanism between MAA and TMP. All energies are reported in kcal/mol. The values in parentheses correspond to reaction enthalpies (ΔH) . Distances shown on the TS complexes are in Å and correspond to bonds being broken or formed at the TS along the reaction path.

The first step on the reaction mechanism involved the coordination of MAA and TMP with RuCl₃ to form the π coordinated complex 7. From 7, MAA and TMP couple to produce intermediate 8 through an oxidative addition transition state (TS7) with an activation Gibbs free energy of 26.9 kcal/mol (energy difference between TS7 and state 7 in Figure 4). Next, intermediate 9 is obtained through a Helimination transition state (TS8) with an activation Gibbs free energy of 7.5 kcal/mol (energy difference between TS8 and state 8 in Figure 4). A reductive elimination transition state (TS9) takes place to generate 10 with an activation Gibbs free energy of 39.8 kcal/mol (energy difference between TS9 and state 9 in Figure 4). Finally, product 5 can be released from 10 regenerating the catalyst. Since the activation Gibbs free energy of the transition state TS9 is the highest among all the transition states (39.8 kcal/mol), the reductive elimination step was shown to be the rate-limiting step in the stepwise mechanism.

In addition to the stepwise mechanism proposed in literature (Scheme 2),14,17,21,22 the concerted mechanism via a polar transition state (Scheme 1) was taken in consideration for the RuCl₃ catalyzed ene reaction (Figure 4, blue path). The first step in the concerted mechanism is the adsorption of MAA on RuCl₃ to form state 11 followed by the formation of the reactant complex 12. The Gibbs activation free energy for the concerted mechanism was 27.4 kcal/mol (energy difference between TS10 and state 11 in Figure 4). When the concerted $(\Delta G^{\ddagger} = 27.4 \text{ kcal/mol})$ and stepwise $(\Delta G^{\ddagger} = 39.8 \text{ kcal/mol})$ mechanisms are compared, the concerted mechanism appears to be kinetically more favorable. TOF calculations were performed, applying the energy span model, confirming the concerted mechanism to be the most favorable with a TOF of 2.09×10^{-2} s⁻¹. To the best of our knowledge, this is the first time that a Ru-catalyzed ene reaction is reported to proceed through a concerted mechanism. However, if one gives a closer look at the reaction profile of Figure 4, it is very likely that the TS7 and TS8 of the stepwise mechanisms are accessible before the TS10 of the concerted mechanism, leading to the highly exothermic state 9 due to formation of HCl in the H-migration step (TS2). In such a case, RuCl₃ will not be an active catalyst since it could decompose due to the formation of HCl. We also tried to locate a TS that involves H-migration to the Ru metal center. However, we found that this H-migration step only takes place involving the Cl atom to form HCl as shown by the IRC calculations.

We next examine the ene reaction between MAA and TMP catalyzed by Ru(II) (RuCl₂·2H₂O) to further address the effect of Ru oxidation state. The stepwise and concerted mechanisms were once again considered. The computed activation and reaction free energies are shown in Figure 5. As in the case of RuCl₃ catalyst, the stepwise mechanism (Figure 5, black path) starts with the coordination of MAA and TMP with RuCl₂· $2H_2O$ to form the π -coordinated complex 15. From 15, MAA

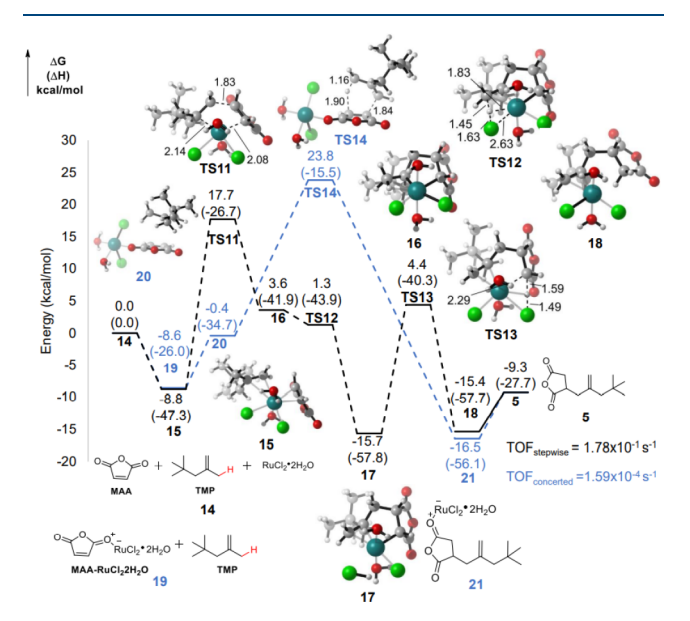


Figure 5. Reaction free energy profile (ΔG) of the stepwise and concerted $RuCl_2 \cdot 2H_2O$ catalyzed ene reaction mechanisms between MAA and TMP. All energies are reported in kcal/mol. The values in parentheses correspond to reaction enthalpies (ΔH) . Distances shown on the TS complexes are in Å and correspond to bonds being broken or formed at the TS along the reaction path.

and TMP couple to produce intermediate 16 through an oxidative addition transition state (TS11) with an activation Gibbs free energy of 26.5 kcal/mol (energy difference between TS11 and state 15 in Figure 5). Next, intermediate 17 is obtained through a H-elimination transition state (TS12). In the energy profile state 16 is higher than TS12, in terms of both Gibbs free energy and enthalpy due to thermal corrections. However, in terms of electronic energies, state 16 is lower in energy than TS12. The nature of TS12 was further confirmed by IRC calculations suggesting that states 16 and 17 are in fact reactant and product of TS12. Following Helimination, a reductive elimination transition state takes place (TS13) to generate 18 with an activation Gibbs free energy of 20.1 kcal/mol (energy difference between TS13 and state 17 in Figure 5). Finally, product 5 can be released from 18 regenerating the catalyst. Since the activation Gibbs free energy of the transition state TS11 is the highest among all the transition states (26.5 kcal/mol), the oxidative addition was found to be the rate-limiting step.

The concerted mechanism (Figure 5, blue path) was also investigated. The Gibbs activation free energy for the concerted mechanism was 32.4 kcal/mol (energy difference between TS14 and state 19 in Figure 5), which is higher than that of the stepwise ($\Delta G^{\ddagger} = 26.5 \text{ kcal/mol}$), making the latter to be kinetically more favorable. TOF calculations confirmed that the stepwise mechanism is the most favorable on RuCl₂· 2H₂O catalyst with a TOF equal to $1.78 \times 10^{-1} \text{ s}^{-1}$ (Figure 5).

By comparing the energy profiles of the RuCl₃ (Figure 4) and RuCl₂·2H₂O (Figure 5) catalyzed ene reaction, it can be observed that the incorporation of MAA into TMP using RuCl₃ will proceed through a concerted mechanism, while RuCl₂·2H₂O proceeds through a stepwise mechanism. In our previous computational study,6 we reported that the uncatalyzed ene reaction between MAA and TMP proceeds through a Gibbs activation free energy of 36.6 kcal/mol. If we compare this result with the results obtained for RuCl₃ (ΔG^{\ddagger} = 27.4 kcal/mol) and RuCl₂·2H₂O ($\Delta G^{\ddagger} = 26.5 \text{ kcal/mol}$) catalysts, it becomes clear that both catalysts will accelerate the incorporation of MAA to TMP. TOF calculations further revealed RuCl₂·2H₂O (1.78 × 10^{-1} s⁻¹) to be a more active catalyst than $RuCl_3(2.09 \times 10^{-2} \text{ s}^{-1})$. Compared to the TOF of AlCl₃ Lewis acid $(4.60 \times 10^{-1} \text{ s}^{-1})$, the RuCl₃·2H₂O catalyst has similar activity to AlCl₃. In addition, we reported a desorption energy of product 5 from AlCl₃ of 16.2 kcal/mol. From Figure 5, we observe that the desorption energy of product 5 from RuCl₂·2H₂O is 7.2 kcal/mol. Thus, even though RuCl₂·2H₂O exhibits comparable TOF to AlCl₃, there is a more favorable (lower) desorption energy of the final product.

Although these results point to the fact that RuCl₂·2H₂O may be a potential catalyst for the ene reaction between MAA and TMP, we note that there is a strong chance that this catalyst decomposes under reaction conditions. This is demonstrated in state 17 where the Ru—Cl distance is 2.83 Å from the formation of HCl through the H-migration TS (TS12). This Ru—Cl distance is larger than that of the RuCl₂·2H₂O (2.31 Å) catalyst. As in RuCl₃, we tried to locate a TS that involved H-migration to the Ru metal center. However, we found that the H-migration proceeds again through involving a Cl atom to form HCl as suggested by the IRC calculations. These results suggest that although the Ru(II) catalyst can be a potential catalyst for the ene reaction between MAA and PIB with a catalytic activity similar to AlCl₃ Lewis

acid, the catalyst may suffer from decomposition under reaction conditions.

In addition to RuCl₃ (Ru(III)) and RuCl₂·2H₂O (Ru(II)), we also considered Ru(0) with the Ru(CO)(P(CH₃))₂ catalytic complex.¹⁷ The stepwise and concerted mechanisms were again investigated as shown in Figure 6. From the

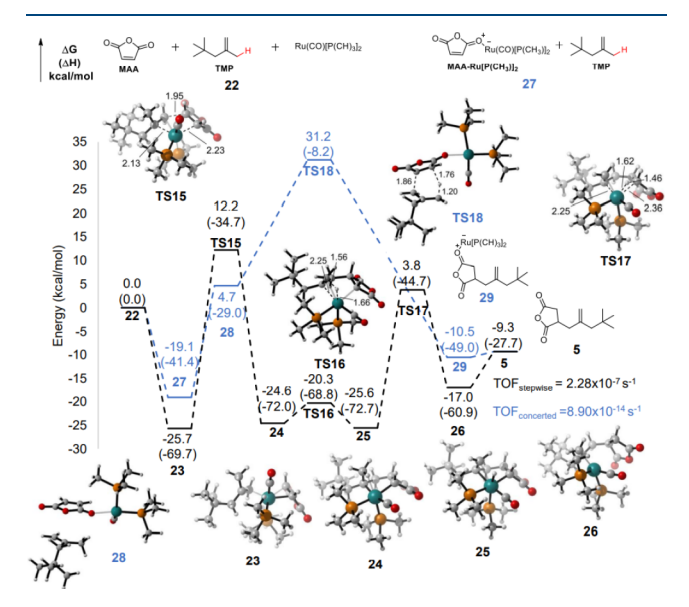


Figure 6. Reaction free energy profile (ΔG) of the stepwise and concerted $Ru(CO)(P(CH_3))_2$ catalyzed ene reaction mechanism between MAA and TMP. All energies are reported in kcal/mol. The values in parentheses correspond to reaction enthalpies (ΔH) . Distances shown on the TS complexes are in Å and correspond to bonds being broken or formed at the TS along the reaction path.

stepwise mechanism (Figure 6, black path) it becomes apparent that the rate-determining step is the oxidative addition with a Gibbs activation free energy of 37.9 kcal/mol (energy difference between TS15 and state 23 in Figure 6). However, in the concerted mechanism (Figure 6, blue path) a Gibbs activation free energy of 50.3 kcal/mol (energy difference between TS18 and state 27 in Figure 6) was obtained. The stepwise mechanism is clearly kinetically more favorable than the concerted. Even though TS15 is under more strain than TS18, as shown by the distortion energy analysis^{28,29} (Figure S4), weaker favorable interactions are observed on TS18 resulting in a larger activation energy when compared to TS15. Interestingly, the activation energy for the $Ru(CO)(P(CH_3))_2$ catalyzed ($\Delta G^{\ddagger} = 37.9 \text{ kcal/mol})$ is higher than the uncatalyzed ($\Delta G^{\ddagger} = 36.6 \text{ kcal/mol}$) ene reaction between MAA and TMP, suggesting that the Ru(CO)(P- $(CH_3)_2$ catalyst does not accelerate the reaction. In addition, a very low TOF was obtained for $Ru(CO)(P(CH_3))_2$ (2.28 × 10^{-7} s^{-1}) compared to RuCl₃ (2.09 × 10^{-2} s^{-1}) and RuCl₂· $2H_2O$ (1.78 \times 10⁻¹ s⁻¹). Summarizing the computational results on the effect of Ru oxidation state on the ene reaction, we revealed Ru(II) to be the most active catalyst with a catalytic activity similar to AlCl₃. However, the stability of RuCl₂·2H₂O catalyst may be an issue under experimental operation, as demonstrated by the significant elongation of the Ru-Cl bond in the H-migration step. The aluminum chloride catalysts will most likely be more stable catalysts than ruthenium chloride. This is further supported by catalyst formation free energy calculations which revealed AlCl₃ to be a

more stable catalyst compared to RuCl₃ (comparison of catalysts at the same oxidation state and type and number of ligands). Specifically, the formation free energy (energy gain considering the reaction: $M + {}^3/{}_2Cl_2 \rightarrow MCl_3$, where M = Al, Ru) of AlCl₃ was -207.2 kcal/mol, whereas that of RuCl₃ was -157.3 kcal/mol at the experimental conditions of 423.15 K.

3.4. Ligand Effects on Ru(II) Catalysts. In an effort to potentially optimize the performance of Ru(II) catalysts on the ene reaction between MAA and PIB, we investigated ligand effects. $CpRuCl^{18,21}$ (Cp=cyclopentadienyl anion) catalyst was first taken into consideration. Again, both the concerted and stepwise mechanisms were investigated. The computed activation and reaction energies are shown in Figure 7. As

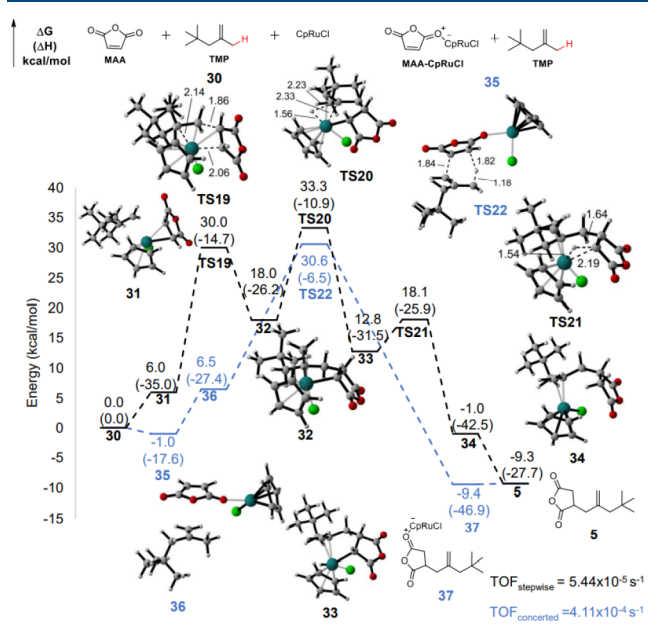


Figure 7. Reaction free energy profile (ΔG) of the stepwise and concerted CpRuCl catalyzed ene reaction mechanism between MAA and TMP. All energies are in kcal/mol. The values in parentheses correspond to reaction enthalpies (ΔH) . Distances shown on the TS complexes are in Å and correspond to bonds being broken or formed at the TS along the reaction path.

discussed above, the stepwise mechanism involved an oxidative addition, H-migration, and reductive elimination steps (Figure 7, black path). From Figure 7, the rate-determining step is the oxidative addition with a Gibbs activation free energy of 30.0 kcal/mol (energy difference between TS19 and state 30). On the other hand, the concerted mechanism was shown to require a Gibbs activation free energy of 31.6 kcal/mol (energy difference between TS22 and state 35 in Figure 7). Although, the stepwise mechanism appears to be kinetically slightly more favorable based on the Gibbs activation free energies, TOF calculations revealed the concerted mechanism to be slightly more favorable pathway (Figure 7). This flipping in the catalytic performance between the two pathways is due to the fact that the energy span model takes into consideration the contribution of states (rate-determining states) rather than assuming that one reaction step (rate-determining step) determines the efficiency of the catalyst.

In addition to CpRuCl catalyst, we considered the $Ru(P(CH_3)_3)_2Cl_2$. The computed activation and reaction energies of the concerted and stepwise mechanisms are shown in Figure 8. In the stepwise mechanism (Figure 8, black path)

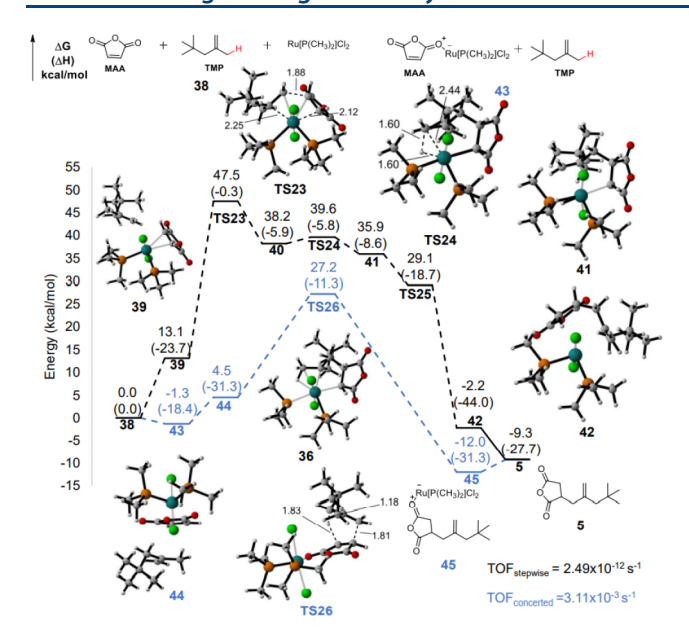


Figure 8. Reaction free energy profile (ΔG) of the stepwise and concerted $\text{Ru}(P(\text{CH}_3)_3)_2\text{Cl}_2$ catalyzed ene reaction mechanism between MAA and TMP. All energies are reported in kcal/mol. The values in parentheses correspond to reaction enthalpies (ΔH) . Distances shown on the TS complexes are in Å and correspond to bonds being broken or formed at the TS along the reaction path.

the rate-determining step is the oxidative addition with a Gibbs activation free energy of 47.5 kcal/mol (energy difference between TS23 and state 38 in Figure 8). On the other hand, the concerted mechanism required a Gibbs activation free energy of 28.5 kcal/mol (energy difference between TS26 and state 43 in Figure 8), which is kinetically more favorable than the stepwise mechanism as shown by the Gibbs activation free energy and confirmed by the TOF calculations (Figure 8). The large activation energy observed in the oxidative addition step can be attributed to a larger strain on TS19 ($\Delta E_{\text{d-total}} = 103.6 \text{ kcal/mol}$) compared to TS22 ($\Delta E_{\text{d-total}} = 46.3 \text{ kcal/mol}$). This is shown in the distortion/interaction energy analysis in Figures S5 and S6. ^{28,29}

Comparing all three Ru(II) catalysts (RuCl₂·2H₂O, CpRuCl, and Ru(P(CH₃)₃)₂Cl₂), we observe that RuCl₂·2H₂O is the most active catalyst as shown by the TOFs (Figure 5, 7 and 8). In addition, the ene reaction proceeds via the stepwise mechanism on RuCl₂·2H₂O (Figure 5), whereas the concerted mechanism is favored in CpRuCl and Ru(P(CH₃)₃)₂Cl₂ catalysts (Figures 7 and 8). To the best of our knowledge, this is the first time that a Ru-catalyzed ene reaction is reported to proceed through a concerted mechanism (i.e., cases of CpRuCl and Ru(P(CH₃)₃)₂Cl₂).

In order to further explore the origin of catalytic activity in the different Ru(II) catalysts, the distortion/interaction energy analysis 28,29 was performed (see Supporting Information). This analysis revealed that the oxidative addition transition state (rate-determining step on the stepwise mechanism) was destabilized, in the case of CpRuCl and Ru(P(CH₃)₃)₂Cl₂, due to larger distortion energies of the catalyst ($\Delta E_{\rm d-cat}=17.8$ kcal/mol and $\Delta E_{\rm d-cat}=27.6$ kcal/mol respectively) when compared to RuCl₂·2H₂O ($\Delta E_{\rm d-cat}=12.0$ kcal/mol) as shown in Figure S5. The larger distortion energies on the catalyst can be attributed to the increase in the size of ligands. However, in the case of the concerted mechanism (Figure S6), there is a decrease in the distortion energy of the catalyst in the case of

CpRuCl ($\Delta E_{d-cat} = 4.4 \text{ kcal/mol}$) and Ru(P(CH₃)₃)₂Cl₂ $(\Delta E_{d-cat} = 1.6 \text{ kcal/mol})$, stabilizing the concerted TS. Although the distortion energies of the RuCl₂·2H₂O catalyst in the concerted (Figure S6) and stepwise mechanisms (Figure S5) are comparable ($\Delta E_{d-cat} = 12.5 \text{ kcal/mol and } \Delta E_{d-cat} = 12.0$ kcal/mol, respectively), the stepwise mechanism is preferred due to stronger interaction energy ($\Delta E_{\text{int}} = -116.1 \text{ kcal/mol vs}$ $\Delta E_{\rm int} = -69.2$ kcal/mol) in the oxidative addition TS. Taken together, our computational study suggests that RuCl₂·2H₂O catalyst kinetically favors the ene reaction between MAA and PIB and the reaction proceeds through a stepwise mechanism due to stronger interaction energy as suggested by the distortion/interaction energy analysis. However, we reiterate here that the stability of RuCl₂·2H₂O catalyst may be an issue as demonstrated by the elongation of the Ru-Cl bond in the H-migration step and the catalyst free energy of formation.

3.5. Catalytic Activity Relationship. In our previous study we developed a catalytic activity relationship showing that stronger adsorption of MAA on the Lewis acid catalyst leads to a lower activation energy. This also leads to a more endothermic desorption of the final product from the catalyst. To elucidate if the correlation between the activation Gibbs free energy and the adsorption energy is a general trend (following a Brønsted–Evans–Polanyi relationship), we plotted the results for Al- and Ru-based catalysts against our previous reported Lewis acid catalysts (i.e., AlCl₃, SnCl₂, TiCl₃, GaCl₃, InCl₃, SnCl₄, and TiCl₄). The correlation plot is shown in Figure 9. We plotted the activation energies of the rate

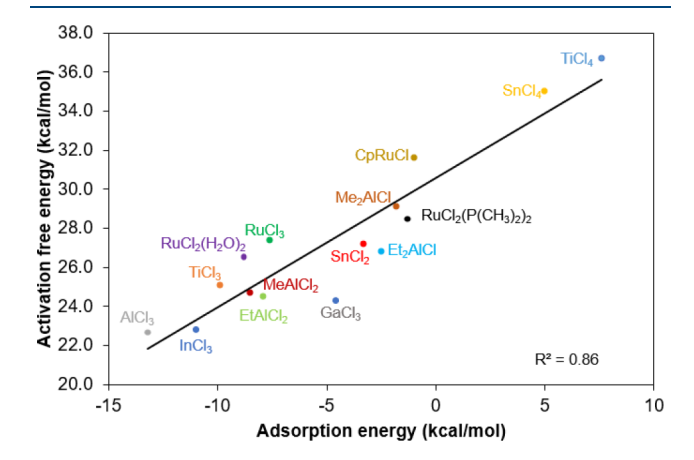


Figure 9. Correlation plot between the activation and the adsorption free energies of the most favorable mechanism (stepwise or concerted).

determining steps taking in consideration the most favorable mechanism (stepwise or concerted). A good correlation ($R^2 = 0.86$) was obtained, suggesting that stronger adsorption of MAA on the catalyst indicates stronger Lewis acidity, leading to lower activation energy. A correlation plot considering the activation and adsorption free energies only for the concerted mechanism was also generated (Figure S7), with the $RuCl_2(H_2O)$ to be an outlier. This is due to the change in the reaction mechanism in the case of $RuCl_2(H_2O)$ favoring the stepwise mechanism instead of the concerted. Overall, Figure 9 demonstrates a clear relationship irrespective of the followed mechanism that governs activity in the Lewis acid catalyzed ene reaction between MAA and PIB.

Relationships and engineering strategies (i.e., ligand and oxidation state modification) like the ones presented in this

work can aid the discovery of industrial catalysts. In addition to this molecular-level understanding of the reaction mechanism, complementary efforts are needed to assess transport effects and accessibility of the active sites to PIB under experimental conditions. Furthermore, detailed microkinetic modeling in concert with molecular dynamics simulations can potentially elucidate the competition between concerted and stepwise mechanisms. This first-principles computational study serves as the first step toward this direction. As such, first-principles-based multiscale modeling can provide insights that may not be accessible by experiments as well as guide lab-scale experimentation in industry.

4. CONCLUSIONS

First-principles calculations and kinetic modeling were performed to explore the catalytic activity of different Al-and Ru-based Lewis acid catalysts on the ene reaction between MAA and PIB. Different alkylaluminum chlorides were taken in consideration (EtAlCl₂, MeAlCl₂, Me₂AlCl, Et₂AlCl) by exploring the concerted mechanism (most favorable pathway). All Al-based catalysts were shown to catalyze the reaction, with the EtAlCl₂ showing an enhanced catalytic activity similar to AlCl₃ (most active Lewis acid catalyst as previously reported⁶). However, desorption of the final product from EtAlCl₂ was found to be less endergonic (more favorable), establishing this alkylaluminum chloride as a promising catalyst for PIBSA formation.

Ru-based catalysts were also explored, with a focus on effects from oxidation state and coordinating ligands on the overall catalytic activity. Both concerted and stepwise mechanisms were investigated. The Ru(II) catalyst (RuCl₂·2H₂O) was revealed to be the most active when compared to Ru(III) $(RuCl_3)$ and Ru(0) $(Ru(CO)(P(CH_3))_2)$, with a catalytic activity comparable to AlCl₃ but with a lower (more favorable) desorption energy of the final product (PIBSA). In addition, our detailed mechanistic analysis unraveled a competition between the concerted and stepwise mechanisms depending on the oxidation state of Ru. In order to further explore the effects of Ru(II) catalyst and address ligand effects on the ene reaction between MAA and PIB, CpRuCl and Ru(P-(CH₃)₃)₂Cl₂ catalysts were considered and compared to (RuCl₂·2H₂O). RuCl₂·2H₂O was found to be the most active catalyst among all three Ru(II) catalysts studied. Interestingly, RuCl₂·2H₂O was found to favor the stepwise mechanism, whereas CpRuCl and Ru(P(CH₃)₃)₂Cl₂ favored the concerted mechanism. To the best of our knowledge, this is the first time that Ru-catalyzed ene reactions are reported to proceed through a concerted mechanism (cases of CpRuCl and $Ru(P(CH_3)_3)_2Cl_2$). Distortion/interaction energy analysis revealed that larger ligands coordinating on Ru destabilize the oxidative addition transition state, disfavoring the stepwise and favoring the concerted mechanism. Although these results suggest RuCl₂·2H₂O to be a potential catalyst for the ene reaction between MAA and PIB, we found that this catalyst may decompose under reaction conditions.

A correlation between the activation and adsorption free energies from the catalysts was obtained, with the latter describing the Lewis acid strength of the catalyst. The activity relationships once again revealed that stronger adsorption of MAA on the Lewis acid catalyst leads to a lower activation energy. Overall, this work demonstrates computational routes to screen different catalysts through ligand engineering and

modification of oxidation states to facilitate energy intense reactions for the chemical industry.

ASSOCIATED CONTENT

Supporting Information

The Supporting Information is available free of charge at https://pubs.acs.org/doi/10.1021/acs.iecr.2c02003.

Energy profiles of Al- and Ru-based catalyzed ene reaction between MAA and PIB, distortion/interaction analysis and Cartesian coordinates and energies of relevant structures (PDF)

AUTHOR INFORMATION

Corresponding Author

Giannis Mpourmpakis — Department of Chemical and Petroleum Engineering, University of Pittsburgh, Pittsburgh, Pennsylvania 15261, United States; orcid.org/0000-0002-3063-0607; Email: gmpourmp@pitt.edu

Authors

Cristian A. Morales-Rivera – Department of Chemical and Petroleum Engineering, University of Pittsburgh, Pittsburgh, Pennsylvania 15261, United States

Glenn Cormack - The Lubrizol Corporation, Wickliffe, Ohio 44092, United States; Occid.org/0000-0002-3537-9247

James Burrington – The Lubrizol Corporation, Wickliffe, Ohio 44092, United States

Nicolas Proust – The Lubrizol Corporation, Wickliffe, Ohio 44092, United States

Complete contact information is available at: https://pubs.acs.org/10.1021/acs.iecr.2c02003

Notes

The authors declare no competing financial interest.

ACKNOWLEDGMENTS

This work has been supported by The Lubrizol Corporation. G.M. acknowledges support by the National Science Foundation (NSF), under Grant 1920623. The authors also acknowledge computational support from the Center for Research Computing (CRC) at the University of Pittsburgh and the Extreme Science and Engineering Discovery Environment (XSEDE), which is supported by the NSF (Grant ACI-1548562).

REFERENCES

- (1) Aleman-Vazquez, L.; Villagómez-Ibarra, J. Polyisobutenylsuccinimides as detergents and dispersants in fuel: infrared spectroscopy application. *Fuel* **2001**, *80* (7), 965–968. Chevalier, Y.; Fixari, B.; Brunel, S.; Marie, E.; De Guio, P. The adsorption of functional polymers from their organic solutions: applications to fuel additives. *Polymer international* **2004**, *53* (5), 475–483. Dubois-Clochard, M.-C.; Durand, J.-P.; Delfort, B.; Gateau, P.; Barré, L.; Blanchard, I.; Chevalier, Y.; Gallo, R. Adsorption of Polyisobutenylsuccinimide Derivatives at a Solid- Hydrocarbon Interface. *Langmuir* **2001**, *17* (19), 5901–5910.
- (2) Pucci, A.; Rausa, R.; Ciardelli, F. Aggregation-Induced Luminescence of Polyisobutene Succinic Anhydrides and Imides. *Macromol. Chem. Phys.* **2008**, 209 (9), 900–906. Pucci, A.; Barsocchi, C.; Rausa, R.; D'Elia, L.; Ciardelli, F. Alder ene functionalization of polyisobutene oligomer and styrene-butadiene-styrene triblock copolymer. *Polymer* **2005**, 46 (5), 1497–1505. Tessier, M.; Maréchal, E. Synthesis of mono and difunctional oligoisobutylenes—III. Modification of α -chlorooligoisobutylene by reaction

- with maleic anhydride. Eur. Polym. J. 1984, 20 (3), 269–280. Rausa, R. Synthesis of polyisobutenyl succinic anhydrides.; product distribution and proposed reaction mechanism. Polym. Prepr. (Am. Chem. Soc., Div. Polym. Chem.) 2007, 48 (2), 227.
- (3) Balzano, F.; Pucci, A.; Rausa, R.; Uccello-Barretta, G. Alder-ene addition of maleic anhydride to polyisobutene: nuclear magnetic resonance evidence for an unconventional mechanism. *Polym. Int.* **2012**, *61* (8), 1256–1262.
- (4) Snider, B. B. Lewis-acid catalyzed ene reactions. Acc. Chem. Res. 1980, 13 (11), 426–432.
- (5) Snider, B. B.; Roush, D. M.; Rodini, D. J.; Gonzalez, D.; Spindell, D. Lewis acid catalyzed reactions of acetylenic esters with alkenes. Stereochemistry and regiochemistry. *J. Org. Chem.* **1980**, 45 (14), 2773–2785.
- (6) Morales-Rivera, C. A.; Proust, N.; Burrington, J.; Mpourmpakis, G. Computational Screening of Lewis Acid Catalysts for the Ene Reaction between Maleic Anhydride and Polyisobutylene. *Ind. Eng. Chem. Res.* **2021**, *60* (1), 154–161.
- (7) Kozuch, S.; Shaik, S. How to conceptualize catalytic cycles? The energetic span model. *Acc. Chem. Res.* **2011**, 44 (2), 101–110.
- (8) Abdelgaid, M.; Dean, J.; Mpourmpakis, G. Improving alkane dehydrogenation activity on γ -Al2O3 through Ga doping. *Catal. Sci. Technol.* **2020**, 10 (21), 7194–7202. Dixit, M.; Kostetskyy, P.; Mpourmpakis, G. Structure-activity relationships in alkane dehydrogenation on γ -Al2O3: site-dependent reactions. *ACS Catal.* **2018**, 8 (12), 11570–11578. Abdelgaid, M.; Mpourmpakis, G. Structure-Activity Relationships in Lewis Acid-Base Heterogeneous Catalysis. *ACS Catal.* **2022**, 12 (8), 4268–4289.
- (9) Kostetskyy, P.; Nolan, C. M.; Dixit, M.; Mpourmpakis, G. Understanding Alkane Dehydrogenation through Alcohol Dehydration on γ-Al2O3. *Ind. Eng. Chem. Res.* **2018**, *57* (49), 16657–16663. Sattler, J. J.; Ruiz-Martinez, J.; Santillan-Jimenez, E.; Weckhuysen, B. M. Catalytic dehydrogenation of light alkanes on metals and metal oxides. *Chem. Rev.* **2014**, *114* (20), 10613–10653. Weckhuysen, B. M.; Schoonheydt, R. A. Alkane dehydrogenation over supported chromium oxide catalysts. *Catal. Today* **1999**, *51* (2), 223–232.
- (10) Karras, M.; Snider, B. B. Alkylaluminum chloride induced cyclization of unsaturated carbonyl compounds. *J. Am. Chem. Soc.* **1980**, *102* (27), 7951–7953. Snider, B. B.; Rodini, D. J.; Karras, M.; Kirk, T. C.; Deutsch, E. A.; Cordova, R.; Price, R. T. Alkylaluminum halides: Lewis acid catalysts which are brønsted bases. *Tetrahedron* **1981**, *37* (23), 3927–3934. Snider, B. B. Synthesis of allylic sulfoxides from alkenes by dichloroethylaluminum catalyzed ene reaction with ptoluenesulfinyl chloride. *J. Org. Chem.* **1981**, *46* (15), 3155–3157. Mikami, K.; Shimizu, M. Asymmetric ene reactions in organic synthesis. *Chem. Rev.* **1992**, *92* (5), 1021–1050.
- (11) Snider, B. B.; Rodini, D. J.; Conn, R. S.; Sealfon, S. Lewis acid catalyzed reactions of methyl propiolate with unactivated alkenes. *J. Am. Chem. Soc.* **1979**, *101* (18), 5283–5293. Snider, B. B.; Duncia, J. V. Stereoselective and regioselective ene reactions of methyl. alphachloroacrylate. *J. Am. Chem. Soc.* **1980**, *102* (18), 5926–5928.
- (12) Snider, B. B. Alkylaluminum Halide Induced Reactions of Carbonyl Compounds with Unactivated Alkenes. In *Selectivities in Lewis Acid Promoted Reactions*; Springer, 1989; pp 147–167.
- (13) Snider, B. B.; Rodini, D. J. Diaklylaluminum chloride catalyzed ene reactions of aldehydes. Synthesis of ipsenol. *Tetrahedron Lett.* **1980**, 21 (19), 1815–1818.
- (14) Trost, B. M.; Indolese, A. F.; Mueller, T. J.; Treptow, B. A Ru catalyzed addition of alkenes to alkynes. *J. Am. Chem. Soc.* **1995**, *117* (2), 615–623.
- (15) Trost, B. M.; Toste, F. D.; Shen, H. Ruthenium-catalyzed intramolecular [5+2] cycloadditions. *J. Am. Chem. Soc.* **2000**, 122 (10), 2379–2380.
- (16) Cho, E. J.; Lee, D. Selectivity in the ruthenium-catalyzed alder ene reactions of di-and triynes. *J. Am. Chem. Soc.* **2007**, *129* (21), 6692–6693. Trost, B. M.; Papillon, J. P.; Nussbaumer, T. Rucatalyzed alkene-alkyne coupling. Total synthesis of amphidinolide P. *J. Am. Chem. Soc.* **2005**, *127* (50), 17921–17937.

- (17) Morita, T.; Akita, M.; Satoh, T.; Kakiuchi, F.; Miura, M. Ruthenium-catalyzed cross-coupling of maleimides with alkenes. *Org. Lett.* **2016**, *18* (18), 4598–4601.
- (18) Trost, B. M.; Roth, G. J. On the Synthesis of Z-γ-Amino-α, β-unsaturated Esters via Ru-Catalyzed Coupling. *Org. Lett.* **1999**, *1* (1), 67–70. Trost, B. M.; Probst, G. D.; Schoop, A. Ruthenium-catalyzed Alder ene type reactions. A formal synthesis of alternaric acid. *J. Am. Chem. Soc.* **1998**, *120* (36), 9228–9236.
- (19) Thompson, M.; Tzoganakis, C.; Rempel, G. A parametric study of the terminal maleation of polypropylene through an Alder Ene reaction. *J. Polym. Sci., Part A: Polym. Chem.* 1998, 36 (13), 2371–2380. Thompson, M. R.; Tzoganakis, C.; Rempel, G. L. Alder Ene functionalization of polypropylene through reactive extrusion. *J. Appl. Polym. Sci.* 1999, 71 (3), 503–516.
- (20) Abbenhuis, R. A.; del Río, I.; Bergshoef, M. M.; Boersma, J.; Veldman, N.; Spek, A. L.; van Koten, G. 16-and 18-Electron Ruthenium (II) Complexes of the Neutral, Potentially Tridentate Triamine Ligand 2, 6-[Bis (dimethylamino) methyl] pyridine (NN 'N). *Inorg. Chem.* 1998, 37 (8), 1749–1758.
- (21) Hong, X.; Trost, B. M.; Houk, K. Mechanism and origins of selectivity in Ru (II)-catalyzed intramolecular (5+ 2) cycloadditions and ene reactions of vinylcyclopropanes and alkynes from density functional theory. *J. Am. Chem. Soc.* **2013**, 135 (17), 6588–6600. Chen, H.; Li, S. Mechanism of ruthenium-catalyzed Alder ene-type reaction: A theoretical study. *Organometallics* **2005**, 24 (5), 872–884.
- (22) Trost, B. M.; Indolese, A. Ruthenium-catalyzed addition of alkenes to acetylenes. *J. Am. Chem. Soc.* **1993**, *115* (10), 4361–4362. Shan, C.; Zhong, K.; Qi, X.; Xu, D.; Qu, L.-B.; Bai, R.; Lan, Y. Long distance unconjugated agostic-assisted 1, 5-H shift in a Ru-mediated alder-ene type reaction: mechanism and stereoselectivity. *Org. Chem. Front.* **2018**, *5* (21), 3178–3185.
- (23) Frisch, M. J.; Trucks, G. W.; Schlegel, H. B.; Scuseria, G. E.; Robb, M. A.; Cheeseman, J. R.; Scalmani, G.; Barone, V.; Mennucci, B.; Petersson, G. A.; Nakatsuji, H.; Caricato, M.; Li, X.; Hratchian, H. P.; Izmaylov, A. F.; Bloino, J.; Zheng, G.; Sonnenberg, J. L.; Hada, M.; Ehara, M.; Toyota, K.; Fukuda, R.; Hasegawa, J.; Ishida, M.; Nakajima, T.; Honda, Y.; Kitao, O.; Nakai, H.; Vreven, T.; Montgomery, J. A., Jr.; Peralta, J. E.; Ogliaro, F.; Bearpark, M.; Heyd, J. J.; Brothers, E.; Kudin, K. N.; Staroverov, V. N.; Kobayashi, R.; Normand, J.; Raghavachari, K.; Rendell, A.; Burant, J. C.; Iyengar, S. S.; Tomasi, J.; Cossi, M.; Rega, N.; Millam, N. J.; Klene, M.; Knox, J. E.; Cross, J. B.; Bakken, V.; Adamo, C.; Jaramillo, J.; Gomperts, R.; Stratmann, R. E.; Yazyev, O.; Austin, A. J.; Cammi, R.; Pomelli, C.; Ochterski, J. W.; Martin, R. L.; Morokuma, K.; Zakrzewski, V. G.; Voth, G. A.; Salvador, P.; Dannenberg, J. J.; Dapprich, S.; Daniels, A. D.; Farkas, Ö.; Foresman, J. B.; Ortiz, J. V.; Cioslowski, J.; Fox, D. J. Gaussian 09, revision D.01; Gaussian Inc.: Wallingford, CT, 2009.
- (24) Legault, C. Y. *CYLview*, version 1.0b; Universitéde Sherbrooke, 2009; http://www.cylview.org (accessed January 2020).
- (25) Zhao, Y.; Truhlar, D. G. The M06 suite of density functionals for main group thermochemistry, thermochemical kinetics, noncovalent interactions, excited states, and transition elements: two new functionals and systematic testing of four M06-class functionals and 12 other functionals. *Theor. Chem. Acc.* 2008, 120 (1), 215–241. Zhao, Y.; Truhlar, D. G. A new local density functional for maingroup thermochemistry, transition metal bonding, thermochemical kinetics, and noncovalent interactions. *J. Chem. Phys.* 2006, 125 (19), 194101.
- (26) Hratchian, H. P.; Schlegel, H. B. Accurate reaction paths using a Hessian based predictor-corrector integrator. *J. Chem. Phys.* **2004**, *120* (21), 9918–9924.
- (27) Bickelhaupt, F. M.; Houk, K. N. Analyzing reaction rates with the distortion/interaction-activation strain model. *Angew. Chem., Int. Ed.* **2017**, *56* (34), 10070–10086.
- (28) Ess, D. H.; Houk, K. Theory of 1, 3-dipolar cycloadditions: distortion/interaction and frontier molecular orbital models. *J. Am. Chem. Soc.* **2008**, *130* (31), 10187–10198.

(29) Bickelhaupt, F.; Houk, K. Distortion/Interaction-Activation Strain Model to Analyze Reaction Rates. Angew. Chem., Int. Ed 2017, 56, 10070.

Recommended by ACS

Influence of Silica-Supported Alkylaluminum on Heterogeneous Zwitterionic Anilinonaphthoquinone Nickel and Palladium-Catalyzed Ethylene Polymerization and C...

Hu Zhang, Zhen Liu, et al.

JULY 25, 2022 ACS CATALYSIS

Synthesis of Unsaturated (Co)polyesters from Ring-Opening Copolymerization by Aluminum Bipyridine Bisphenolate **Complexes with Improved Protonic Impurities Tolerance**

Xiao-Lu Chen, Yue-Sheng Li, et al.

APRIL 19, 2022

MACROMOLECULES

READ 🗹

Multifunctional Catalysts for Ring-Opening Copolymerizations

Claire A. L. Lidston, Geoffrey W. Coates, et al.

AUGUST 26, 2022 ACS CATALYSIS

READ 🗹

Copolymerization of Ethylene and Long-Chain Functional α -**Olefins by Dinuclear Zirconium Catalysts**

Jessica Sampson, Theodor Agapie, et al.

JUNE 07, 2021

ORGANOMETALLICS

READ 🗹

Get More Suggestions >